

Preprint of

Exploring the Limits of Polarization Transfer Efficiency in Homonuclear Three Spin Systems

J. L. Neves, B. Heitmann, T. O. Reiss, H. H. R. Schor, N. Khaneja, S. J. Glaser

J. Magn. Reson. 181, 126-134 (2006).

Exploring the Limits of Polarization Transfer Efficiency in Homonuclear Three Spin Systems

March 14, 2006

Jorge L. Neves^{a,b}, Björn Heitmann^a, Timo O. Reiss^a, Heloiza H. R. Schor^b,
Navin Khaneja^c, Steffen J. Glaser^{a,*}

^a Chemistry Department, Technische Universität München, 85747 Garching, Germany

^b Departamento de Química, ICEx, UFMG 31270-901 Belo Horizonte, MG, Brazil

^c Division of Applied Sciences, Harvard University, Cambridge, MA 02138, USA

Abstract

The limits of polarization transfer efficiency are explored for systems consisting of three isotropically coupled spins 1/2 in the absence of relaxation. An idealized free evolution and control Hamiltonian is studied, which provides an upper limit of transfer efficiency (in terms of transfer amplitude and transfer time) for realistic homonuclear spin systems with arbitrary Heisenberg-type coupling constants J_{12} , J_{13} , and J_{23} . It is shown that optimal control based pulse sequences have significantly improved transfer efficiencies compared to conventional transfer schemes. An experimental demonstration of optimal polarization transfer is given for the case of the carbon spin system of fully ^{13}C labelled alanine at low magnetic field.

* Corresponding author.

E-mail address: glaser@ch.tum.de (S. J. Glaser)

1 Introduction

Polarization transfer between coupled spins forms the basis of many two-dimensional experiments [1]. Although a large number of pulse sequences have been developed to effect transfer of polarization or coherence, many fundamental questions of both theoretical and practical interest are still open. Here we address the problem of optimal transfer efficiency in systems consisting of three isotropically coupled spins $1/2$ in the absence of relaxation. This scenario is relevant for homonuclear spin systems in liquid state NMR, where the coupling between spins is characterized by isotropic (Heisenberg-type) coupling terms [1, 2], see Theory section. Here, we use the term transfer efficiency to reflect both the transfer amplitude and the required transfer time [2]. Ideally, the transfer amplitude should be as large as possible and the transfer time should be as short as possible, in order to reduce relaxation losses. It is well known that in systems consisting of two homonuclear spins $1/2$, TOCSY-type (*Total Correlation Spectroscopy*) transfer experiments [3-5] are faster and hence more efficient than COSY-type (*Correlation Spectroscopy*) experiments [6]. TOCSY sequences are designed to suppress offset terms and to create isotropic mixing conditions. For an isolated pair of spins $1/2$, free evolution under the effective isotropic mixing Hamiltonian results in complete polarization transfer during a mixing time of $1/(2J_{12})$, where J_{12} is the coupling constant between the two spins.

For spin systems consisting of three or more coupled spins, the situation is more complicated. Here, the TOCSY transfer efficiency strongly depends on the relative size of the coupling constants [2, 5, 7-9]. For example, under isotropic mixing conditions, the transfer efficiency between two spins with a direct coupling constant J_{12} is very inefficient if the coupling constants J_{13} and J_{23} to a third spin have twice the magnitude and the opposite sign of the direct coupling, i.e. if $J_{13} \approx J_{23} \approx -2J_{12}$ [2, 7]. One of the first approaches to improve the transfer efficiency and to exert some control over the evolution was based on selective mixing sequences [2, 5, 10-23], which (in contrast to TOCSY) are also known as TACSYS (*Tailored Correlation Spectroscopy*) experiments [2, 5]. The polarization transfer properties of the large number of suggested TOCSY and TACSYS experiments can be conveniently classified based on the corresponding effective coupling topologies. It was shown that selective TACSYS transfer is always more efficient than TOCSYS transfer, if the magnitude of at least one of the indirect couplings ($|J_{13}|$ or $|J_{23}|$) is smaller than the magnitude of the direct coupling $|J_{12}|$. If the magnitudes of both indirect couplings to a third spin are significantly larger than the magnitude of the direct coupling between the two spins of interest (i.e. $|J_{13}/J_{12}| \approx |J_{23}/J_{12}| > 2$), in most cases a two-step sequential TACSYS transfer via the third spin is more efficient. TOCSYS transfer

is superior to TACSY and sequential TACSY transfer only if the indirect couplings are large and have the same sign as the direct coupling between the spin pair of interest ($J_{13}/J_{12} \approx J_{23}/J_{12} > 2$) [2, 5]. However, conventional COSY-, TOCSY-, and TACSY-type sequences are only specific examples and do not represent the most general type of polarization transfer experiments.

The goal of this paper is to explore the physical limits of polarization transfer efficiency and to compare these limits with the efficiency of conventional experiments. Such theoretical limits provide an important benchmark for all present and future pulse sequences. On the one hand they show in which cases these limits are already reached by conventional experiments and hence where all additional efforts to find further improvements in transfer efficiency would be futile. On the other hand, they show where conventional approaches are far from the optimum and where it is worth to invest in the development of better practical pulse sequences. Finding the most efficient polarization transfer sequence is a problem in optimal control [24]. So far, an analytical characterization of optimal transfer efficiency is only known for the case of isolated two-spin systems [25-27]. Here, we use the optimal-control based numerical optimization algorithm (GRAPE) [28], which has previously been successfully used for a large number of applications, including broadband pulses [29-32], pattern pulses [33], solid-state NMR applications [34-36], logical gates for quantum information processing [28, 37] and relaxation-optimized coherence transfer [28]. Similar numerical algorithms have been applied in the study of laser control of molecular vibrations and reactions [38-44] and for the design of band-selective pulses in MRI applications [45-47]. For the case of two coupled spins in the absence of relaxation, it has been demonstrated that the pulse sequences found by the GRAPE algorithm closely approach the analytically derived physical limits [25, 27, 28]. Here, we use the GRAPE algorithm to explore the limits of polarization transfer in isotropically coupled three-spin systems.

2 Theory

We focus on polarization transfer $I_{1z} \rightarrow I_{2z}$ between two spins that are part of a system consisting of three spins 1/2 in the absence of relaxation. The state of the spin system is characterized by the density operator $\rho(t)$, and its equation of motion is the Liouville-von Neuman equation [1]

$$\dot{\rho}(t) = -i [(\mathcal{H}_o + \sum_{k=1}^M u_k(t)\mathcal{H}_k), \rho(t)], \quad (1)$$

where \mathcal{H}_o is the free evolution Hamiltonian, \mathcal{H}_k correspond to control fields and $u_1(t), u_2(t), \dots, u_M(t)$ represent the control amplitudes that can be varied as a function of time. In practice, the free evolution Hamiltonian for a system of three coupled homonuclear spins in isotropic solution is

$$\mathcal{H}_o^{real} = \mathcal{H}_{iso} + \mathcal{H}_{off} \quad (2)$$

with the isotropic coupling term

$$\mathcal{H}_{iso} = \sum_{m < n} 2\pi J_{mn} (I_{mx}I_{nx} + I_{my}I_{ny} + I_{mz}I_{nz}) \quad (3)$$

and the offset term

$$\mathcal{H}_{off} = \sum_{m=1}^3 2\pi\nu_m I_{mz}. \quad (4)$$

The isotropic coupling represented by \mathcal{H}_{iso} is also known as Heisenberg coupling. Experimentally, in homonuclear spin systems only two control amplitudes ($u_x(t)$ and $u_y(t)$) are available, which correspond to x or y pulses applied simultaneously to *all* spins:

$$\mathcal{H}_{control}^{real} = 2\pi u_x(t) \sum_{m=1}^3 I_{mx} + 2\pi u_y(t) \sum_{m=1}^3 I_{my}. \quad (5)$$

In the limit of identical offsets ($\nu_1 = \nu_2 = \nu_3$), no selective rotations of the individual spins are possible. However, if the three spins have different offsets, selective rotations are possible. In order to explore the limits of transfer efficiency, we first focus on the following idealized setting (which in practice can only be approximated), where we assume that arbitrarily fast selective pulses can be selectively applied to the individual spins and where the chemical shifts of the spins have already been eliminated in a first averaging process. The corresponding free evolution and control terms of this idealized Hamiltonian are given by

$$\mathcal{H}_o^{ideal} = \mathcal{H}_{iso} \quad (6)$$

and

$$\mathcal{H}_{control}^{ideal} = 2\pi \sum_{m=1}^3 \{u_{mx}(t)I_{mx} + u_{my}(t)I_{my}\}. \quad (7)$$

Hence, in this idealized setting, the six control amplitudes

$$u_1(t) = u_{1x}(t), u_2(t) = u_{1y}(t), u_3(t) = u_{2x}(t), u_4(t) = u_{2y}(t), u_5(t) = u_{3x}(t), u_6(t) = u_{3y}(t) \quad (8)$$

are assumed to be available.

Now we consider the problem to find the optimal amplitudes that steer a given initial density operator $\rho(0) = I_{1z}$ in a specified time τ to a density operator $\rho(\tau)$ with maximum overlap to the

target operator I_{2z} . For any given control sequence, the normalized polarization transfer amplitude $T_{12}(\tau)$ for the transfer $I_{1z} \rightarrow I_{2z}$ can be defined as [2, 5]

$$T_{12}(\tau) = \frac{1}{2} \text{tr}\{I_{2z}\rho(\tau)\}. \quad (9)$$

In the GRAPE optimizations [28] of the pulse sequences (represented by the control amplitudes $u_k(t)$), the transfer time τ is discretized in finite time intervals Δt and during each interval the control amplitudes are constant, e.g. during the j^{th} step the amplitude $u_k(t)$ of the k^{th} control Hamiltonian is given by $u_k(j)$. For each transfer time τ , the transfer amplitude $T_{12}(\tau)$ is maximized using the gradient [28]

$$\frac{\delta T_{12}(\tau)}{\delta u_k(j)} = -i \Delta t \text{tr}\{\mathcal{H}_k [\rho_j, \lambda_j]\}, \quad (10)$$

where $\lambda(\tau) = I_{2z}$ and the time evolutions of the density operator $\rho(t)$ and of the backward propagated target operator $\lambda(t)$ are governed by the same equation of motion (Eq. 1). Starting from random functions $u_k(t)$, the control amplitudes were optimized using a conjugate gradient algorithm based on Eq. (10) [28]. For the coupling constants $J_{13} = J_{23} = -2.4J_{12}$, Fig. 1 shows an example of optimized control amplitudes $u_1(t) = u_{1x}(t), \dots, u_6(t) = u_{3y}(t)$ for a transfer time $\tau = 0.32J_{12}^{-1}$.

We denote the graphical representation of the maximum achievable transfer amplitude $T_{12}(\tau)$ as the TOP (time optimal pulse) curve [27]. An example of a numerically optimized TOP curve is shown in Fig. 2 (solid curve) for the case $J_{13} = J_{23} = -2.4J_{12}$.

The minimum time τ^* for which the maximum transfer amplitude T_{12} is achieved is a function of the coupling constants [27]. If $J_{12} \neq 0$ or if both J_{13} and J_{23} are non-zero, the spin system is fully controllable and the maximum transfer amplitude is $T_{12}(\tau^*) = 1$, corresponding to the unitary bound [48, 49].

As a convenient measure for the efficiency of polarization transfer between spins I_1 and I_2 in terms of transfer *amplitude* and *duration*, here we use the standard transfer efficiency η defined as [2, 5]

$$\eta = \max_{\tau > 0} \left\{ T_{kl}(\tau) \exp(-\tau |J_{12}|) \right\}. \quad (11)$$

This transfer efficiency η represents the maximum of the exponentially damped TOP curve (c.f. dashed curve in Fig. 2), where the damping constant $\tau_{damp} = |J_{12}|^{-1}$ corresponds to (twice) the ideal TOCSY transfer time that would be found if spins I_1 and I_2 would form an *isolated* pair of coupled spins. (For alternative definitions of transfer efficiency, see [2].) The time for which the damped TOP curve achieves its maximum is denoted as τ_{max} . It can be conveniently determined numerically

and is similar to (but cannot exceed) τ^* defined above. Note that η and τ_{max} depend only on the relative coupling constants J_{13}/J_{12} and J_{23}/J_{12} [2]. Hence for a general three-spin system, both $\eta(J_{13}/J_{12}, J_{23}/J_{12})$ and $\tau_{max}(J_{13}/J_{12}, J_{23}/J_{12})$ can be represented by two-dimensional contour plots.

3 Transfer Efficiency Maps

For $-5.2 \leq J_{13}/J_{12} \leq 5.2$ and $-5.2 \leq J_{23}/J_{12} \leq 5.2$, we calculated $53 \times 53 = 2809$ TOP curves using the optimal control based GRAPE algorithm [28]. For each TOP curve, the resulting transfer efficiency η (c.f. Eq. 11 and Fig. 2) was determined and the resulting optimal control based η^{OC} map is shown in Fig. 3A. For comparison, the transfer efficiency map η^{TOCSY} of isotropic mixing [3, 5, 7] is shown in Fig. 3B. Fig. 3C shows the (constant) transfer efficiency $\eta^{TACSY} = 0.622$ of a (*IOO*-type) TACSY experiment [2, 5], where the couplings to spin I_3 are effectively eliminated, resulting in the isotropic mixing transfer dynamics of an isolated two-spin system. Fig. 3D shows the best transfer efficiency $\eta^{two-step}$ achievable by a two-step sequential TACSY transfer consisting of a selective (*OIO*-type TACSY) isotropic mixing transfer between spins I_1 and I_3 (while decoupling spin I_2) followed by a selective (*OOI*-type TACSY) isotropic mixing transfer between spins I_3 and I_2 (while decoupling spin I_1) [2, 5]. Cross sections along the lines $J_{13} = J_{23}$ and $J_{13} = -J_{23}$ of these efficiency maps are shown in Fig. 4. As expected, for all combinations of coupling constants, η^{OC} was found to be at least as large as η^{TOCSY} , η^{TACSY} , and $\eta^{two-step}$. In the case of isotropic mixing, the transfer efficiency η^{TOCSY} reaches η^{OC} only in the special case where $J_{13} = J_{23} = 0$ and also closely approaches η^{OC} for $J_{13} = J_{23} \approx 4J_{12}$. However, for most combinations of coupling constants, η^{TOCSY} is significantly smaller than η^{OC} . If the magnitude of at least one of the indirect couplings ($|J_{13}|$ or $|J_{23}|$) is on the order of or smaller than $|J_{12}|$, we find $\eta^{OC} = \eta^{TACSY}$. Hence, for small indirect couplings, the single-step TACSY transfer turns out to be the optimal transfer strategy. On the other hand, in the limit where both indirect couplings are significantly larger than the direct coupling, the two-step TACSY transfer approaches the optimum transfer efficiency.

The symmetry properties of the conventional sequences have been previously discussed in detail [2, 5]. The only symmetry element found in the η^{OC} map is a trivial reflection symmetry around the diagonal ($J_{13} = J_{23}$). This is a direct result of the fact that for any pulse sequence with a transfer amplitude $T_{12}(t)$ from I_{1z} to I_{2z} , the time-reversed pulse sequence will provide the same transfer amplitude from I_{2z} to I_{1z} , i.e. $T_{21}(t) = T_{12}(t)$.

The optimal transfer time τ_{max} for the damped TOP curve is shown in Fig. 5 as a function of J_{13}/J_{12} and J_{23}/J_{12} . If the magnitude of one of the indirect coupling constants is smaller than the magnitude of the direct coupling, the transfer time is identical to the transfer time of the TACSY experiment. However, if the magnitudes of both indirect coupling constants are larger than $|J_{12}|$, the optimal transfer time is markedly reduced.

4 Experimental

The presented theoretical limits of polarization transfer are relevant for many applications of practical interest. For example in biological applications, homonuclear spin systems consisting of three coupled ^1H spins occur in proteins and nucleic acids. For such practical applications, the idealized model considered here can provide only upper bounds for the largest achievable transfer efficiency because additional constraints have to be taken into account. (I) The fidelity and duration of spin-selective pulses depends on the size of chemical shift difference in a given spin system. For small or vanishing chemical shift differences (e.g. between geminal protons), spin-selective control is very limited or even impossible. (II) In most practical applications, pulse sequences are required that work not only for a given spin system with known chemical shifts but that cover finite chemical shift ranges typically found in specific applications. (III) In many applications, typical ranges of coupling constants need to be taken into account. (IV) The sequences should be robust with respect to typical variations of rf amplitudes due to imperfect pulse calibration and rf inhomogeneity. (V) Optimal pulse sequence performance requires high standards for spectrometer hardware with respect to pulse switching time, linear amplifiers and constant rf power during long irradiation periods. (VI) Based on results for heteronuclear spin systems [52-55], it is expected that experiments optimized for the specific relaxation properties of a given sample may have the best sensitivity. (VII) In many experimental settings, spin systems consisting of more than three coupled spins are relevant.

Consideration of all these issues is beyond the scope of this paper and require further studies to yield pulse sequences for practical applications. In this section, we demonstrate how some of these problems (I, II, IV, V) can be addressed and present an experimental example illustrating on the one hand the relation between ideal and practical pulse sequences and on the other hand significant gains compared to conventional approaches.

For an experimental demonstration of optimal control based polarization-transfer sequences,

we chose fully ^{13}C labelled alanine as a model compound. At low field (62.5 MHz ^{13}C Larmour frequency) the offset differences of the C_β , C' , and C_α resonances are large enough (on the order of kHz) to allow for fast spin-selective rotations. On the other hand, effective isotropic mixing conditions can be approximated because the offset frequencies are smaller than the available rf amplitude. Alanine was dissolved in D_2O and the experiments were performed at a temperature of 27°C using a Bruker AC 250 spectrometer with modern SGU units for rf control. The ^1H spins were decoupled and the nuclear spins of C_β , C' , and C_α correspond to I_1 , I_2 , and I_3 , respectively. In this isotropically coupled three-spin system, the experimentally determined coupling constants are $J_{12} = -1.6$ Hz, $J_{13} = 33.7$ Hz, and $J_{23} = 59.6$ Hz. For this combination of coupling constants, the numerically determined ideal TOP curve for polarization transfer from spin I_1 (C_β) to I_2 (C') is shown in Fig. 6 A (solid curve), assuming six independent and unlimited control amplitudes, c.f. Eqs. (7) and (8), which were digitized in steps of $30 \mu\text{s}$. The minimum time to achieve full polarization transfer is $\tau^* \approx 18.9$ ms. This is about 20% shorter than the total transfer time of an ideal sequential two-step TACSy sequence, which requires a minimum transfer time of $1/(2J_{13}) + 1/(2J_{23}) = 23.2$ ms for complete transfer [2].

In our experiments, the ^{13}C transmitter frequency was set in the center between the C_β and C' resonance frequencies, resulting in offsets $\nu_1 = -4941.7$ Hz, $\nu_2 = 4941.7$ Hz, and $\nu_3 = -2837.7$ Hz. For these offset frequencies, we also calculated the more realistic TOP curve (dashed curve in Fig. 6 A), assuming only the two non-selective and unlimited control amplitudes u_x and u_y , c.f. Eq. (5). Here the minimum time to achieve full polarization transfer is $\tau^* \approx 20.7$ ms. Due to the relatively large offset differences in the alanine spin system, the TOP curve based on non-selective pulses closely approaches the ideal TOP curve.

In practice, rf amplitudes are not unlimited and pulse sequences should be robust with respect to rf inhomogeneity and variations of chemical shifts [28]. We therefore also optimized five purely phase-modulated pulse sequences (with durations τ of 19.9 ms, 26.7 ms, 28.4 ms, 39.8 ms, and 56.8 ms) with a constant rf amplitude $\sqrt{u_x^2 + u_y^2}$ of 10.125 kHz for offset ranges $\nu_1 = -4941.7 \pm 170$ Hz, $\nu_2 = 4941.7 \pm 170$ Hz, and $\nu_3 = -2837.7 \pm 170$ Hz and a Gaussian rf amplitude distribution with a full width at half height of 10 %. The resulting pulse shapes are available for download in Bruker format on the website www.org.chemie.tu-muenchen.de/glaser. For example, the phase modulation $\varphi(t)$ of the optimized sequence with a duration of 19.9 ms is shown in Fig. 7A. In Fig. 6 A, the resulting transfer amplitudes (averaged over all combinations of offsets and rf amplitudes for

which polarization transfer was optimized) are represented by solid circles. The maximum transfer amplitude of 0.97 is reached for a mixing time of about 26.7 ms. As expected, the ideal TOP curve for six selective control fields (solid curve) forms an upper bound for the more realistic TOP curve for two non-selective control fields, which in turn forms an upper bound for the transfer amplitudes of the robust practical sequences (solid circles).

Experimental polarization transfer amplitudes were measured using standard procedures [5]. The initial density operator $\rho(0) = I_{1z}$ was prepared by complete saturation of the ^{13}C spins followed by selective heteronuclear Hartmann-Hahn transfer from H_β to C_β [50, 51] and a 90°_y pulse that flips I_{1x} to I_{1z} . After applying a polarization transfer sequence of duration τ to $\rho(0)$, the resulting polarization I_{2z} (C') is rotated to I_{2x} by a 90°_y pulse and a spectrum is recorded. Sections of experimental spectra showing the C' signal for the optimized pulse sequences are shown in Fig. 6 B (solid curves). The normalized experimental transfer amplitude T_{12} is given by the integrated signal intensity of spin I_2 divided by the integrated signal intensity of spin I_1 which results if a 90°_y pulse is applied directly to $\rho(0) = I_{1z}$. In Fig. 6 A, the experimental polarization transfer amplitudes between spins I_1 (C_β) and I_2 (C') resulting from the optimized practical pulse sequences are represented by open circles. A reasonable match is found between experimental (open circles) and simulated (solid circles) polarization transfer amplitudes. The remaining discrepancies can be attributed to experimental imperfections and relaxation effects which were not taken into account in the present simulations.

For comparison, Fig. 6 A also shows simulated (solid squares) and experimental (open squares) transfer amplitudes for the alanine spin system under the TOCSY sequence DIPSI-2 [56] with the same rf amplitude of 10.125 kHz as used for the optimal control based sequences. In Fig. 6 B the C' signal (dashed curves) is shown as a function of the mixing time. For this rf amplitude, the cycle time of DIPSI-2 is 2.84 ms and the periodic phase modulation of seven DIPSI-2 cycles corresponding to a total mixing time of 19.9 ms is shown in Fig. 7B. In order to guide the eye, in Fig. 6 A the simulated transfer amplitudes (solid squares) for integer multiples of the cycle time were connected by a smooth curve using a cubic spline fit (dash-dotted curve). Again, a reasonable match is found between simulated and experimental DIPSI-2 transfer functions $T_{12}(\tau)$, which show two pronounced maxima at $\tau = 19.9$ ms and $\tau = 39.8$ ms. For these two maxima, the simulated (and experimental) transfer amplitudes are 0.61 (0.62) and 0.66 (0.64). In comparison, the corresponding simulated (and experimental) transfer amplitudes of the optimized practical pulse sequence with durations

$\tau = 19.9$ ms and $\tau = 39.8$ ms are 0.82 (0.80) and 0.97 (0.89), respectively. Hence, in the simulations (experiments) at $\tau = 19.9$ ms a gain of 34 % (29 %) is found and at $\tau = 39.8$ ms a gain of 47 % (39%).

5 Discussion

The tools of optimal control make it possible to explore the limits of polarization transfer in non-trivial spin systems. Although the GRAPE algorithm is not guaranteed to converge to a globally optimal pulse shape, experience with cases where analytical solutions are known [28] suggests that the presented efficiency maps not only provide the currently best known transfer efficiencies but also closely approach the theoretical limits. On the one hand, the presented results provide a benchmark for all known or future pulse sequences. On the other hand, they motivate the search for a detailed analytical characterization of the optimal transfer strategy. The presented results for polarization transfer $I_{1z} \rightarrow I_{2z}$ also apply to transfer of in-phase coherence $I_{1x} \rightarrow I_{2x}$ or $I_{1y} \rightarrow I_{2y}$ because e.g. I_{1x} can be flipped to I_{1z} by a hard pulse which takes a negligible amount of time. For cases where the optimal efficiency is larger than the single-step TACSY transfer, a different optimal pulse sequence corresponds to each combination of relative coupling constants J_{13}/J_{12} and J_{23}/J_{12} . This also motivates the search for optimal pulse sequences for ranges of relative coupling constants and chemical shift ranges that are characteristic for specific applications. For example, homonuclear spin systems in proteins and nucleic acids are candidates for more efficient polarization-transfer experiments to establish chemical shift correlations and to quantify couplings. For such applications, the presented transfer efficiencies form an upper limit for practical pulse sequences which must rely on chemical shift differences to effect selective rotations of individual spins. This was demonstrated theoretically and experimentally for the ^{13}C spin system of fully ^{13}C labelled alanine, where we also designed pulse sequences that are robust with respect to realistic rf inhomogeneities and variations of chemical shifts. Significant gains in polarization transfer amplitude were found compared to conventional TOCSY experiments, opening new avenues for efficient tailor-made homonuclear polarization transfer experiments. A characteristic of optimal control-based pulse sequences is that they do not consist of a basic pulse sequence which is repeated throughout the entire mixing time as in conventional TOCSY experiments, c.f. Fig. 7 A and B [3-5]. Instead, at each point in time the optimum pulse is applied to steer the spin system to the desired target state. In this study, we did not take specific relaxation mechanisms into account, to explore the limits of homonuclear time-optimal polarization

transfer in the most general setting. However, similar to the case of heteronuclear experiments [52-55], it is expected that the development of homonuclear relaxation-optimized transfer schemes will lead to further improved pulse sequences.

Acknowledgments J.L.N. acknowledges a DAAD-CAPES scholarship. S.J.G. thanks the Deutsche Forschungsgemeinschaft for grants Gl 203/4-2. N.K. acknowledges support by grants ONR 38A-1077404, AFOSR F9550-05-1-0443 and AFOSR FA9550-04-1-0427.

References

- [1] R. R. Ernst, G. Bodenhausen, A. Wokaun, *Principles of Nuclear Magnetic Resonance in One and Two Dimensions*, (Clarendon Press, Oxford, 1987).
- [2] S. J. Glaser, Coupling topology dependence of polarization-transfer efficiency in TOCSY and TACSU experiments, *J. Magn. Reson. A* **104**, 283-301 (1993).
- [3] L. Braunschweiler and R. R. Ernst, Coherence transfer by isotropic mixing: Application to proton correlation spectroscopy, *J. Magn. Reson.* **53**, 521 (1983).
- [4] A. Bax and D. G. Davis, MLEV-17-based two-dimensional homonuclear magnetization transfer spectroscopy, *J. Magn. Reson.* **65**, 355 (1985).
- [5] S. J. Glaser and J. J. Quant, Homonuclear and heteronuclear Hartmann-Hahn transfer in isotropic liquids, in "Advances in Magnetic and Optical Resonance" (W. S. Warren, Ed.), Vol. 19, pp. 59 - 252, Academic Press, San Diego, 1996.
- [6] W. P. Aue, E. Bartholdi, R. R. Ernst, Two-dimensional spectroscopy. Application to nuclear magnetic resonance, *J. Chem. Phys.* **64**, 2229-2246 (1999).
- [7] O. Schedletsky and S. J. Glaser, Analytical coherence-transfer functions for the general AMX spin system under isotropic mixing, *J. Magn. Reson. A* **123**, 174-180 (1996).
- [8] B. Luy, O. Schedletsky, and S. J. Glaser, Analytical polarization transfer functions for four coupled spins 1/2 under isotropic mixing conditions, *J. Magn. Reson.* **138**, 19-27 (1999).
- [9] S. C. Sahu, Analysis and prediction of isotropic mixing magnetization transfer profiles in three-spin topologies, *J. Magn. Reson.* **147**, 121-128 (2000).

- [10] A. Bax and D. G. Davies, Homonuclear Hartmann-Hahn magnetization transfer: New one- and two-dimensional NMR methods for structure determination and spectral assignment, In "Advanced Magnetic Resonance Techniques in Systems of High Molecular Complexity" (N. Nicolai and G. Valensin, eds.). Birkhäuser, Boston, 1986.
- [11] S. J. Glaser and G. Drobny, The tailored TOCSY experiment: Chemical shift selective coherence transfer, *Chem. Phys. Lett.* **164**, 456-462 (1989).
- [12] S. J. Glaser and G. P. Drobny, Controlled coherence transfer by a multiple-step tailored TOCSY experiment, *Chem. Phys. Lett.* **184**, 553-559 (1991).
- [13] A. Mohebbi, A. J. Shaka, Selective homonuclear cross polarization *J. Magn. Reson.* **94**, 204-208 (1991).
- [14] R. Konrat, I. Burghardt, G. Bodenhausen, Coherence transfer in nuclear magnetic resonance by selective homonuclear Hartmann-Hahn correlation spectroscopy, *J. Am. Chem. Soc.* **113**, 9135-9140 (1991).
- [15] Ě. Kupče and R. Freeman, Multiple Hartmann-Hahn coherence transfer in nuclear magnetic resonance, *J. Am. Chem. Soc.* **114**, 10671-10672 (1992).
- [16] E. Kupče and R. Freeman, Stepwise propagation of coherence along a chain of atoms: DAISY-2, *J. Magn. Reson.* **100**, 208-214 (1992).
- [17] P. Schmidt, H. Schwalbe, S. J. Glaser and C. Griesinger, Exclusive Tailored Correlation Spectroscopy (E.TACS), *J. Magn. Reson. B* **101**, 328-332 (1993).
- [18] J. Quant, T. Prasch, S. Ihringer and S. J. Glaser, Tailored Correlation Spectroscopy for the Enhancement of Fingerprint Cross Peaks in Peptides and Proteins, *J. Magn. Reson. B* **106**, 116-121 (1995).
- [19] A. Majumdar and E. R. P. Zuiderweg, Efficiencies of double- and triple-resonance J cross polarization in multidimensional NMR, *J. Magn. Reson. A* **113**, 19-31 (1995).
- [20] D. Abramovich, S. Vega, J. Quant and S. J. Glaser, The Floquet description of TOCSY and E.TACS experiments, *J. Magn. Reson. A* **115**, 222-229 (1995).
- [21] J. Huth and G. Bodenhausen, Suppression of passive scalar couplings in doubly selective coherence transfer, *J. Magn. Reson. A* **114**, 129-131 (1995).

- [22] T. Carlomagno, M. Maurer, M. Sattler, M. G. Schwendinger, S. J. Glaser, and C. Griesinger, PLUSH TACSy: Homonuclear planar TACSy with two-band selective shaped pulses applied to $C_{\alpha}C'$ transfer and C_{β} , $C^{aromatic}$ correlations, *J. Biomol. NMR* **8**, 161-170 (1996).
- [23] E. R. P. Zuiderweg, L. Zeng, B. Brutscher, R. C. Morshauer, Band-selective hetero- and homonuclear cross-polarization using trains of shaped pulses, *J. Biomol. NMR* **8**, 147-160 (1996).
- [24] A. Bryson, Jr., Y.-C. Ho, Applied optimal control, Hemisphere, Washington, D.C. (1975).
- [25] N. Khaneja, R. Brockett, S. J. Glaser, Time optimal control in spin systems, *Phys. Rev. A* **63**, 032308/1-13 (2001).
- [26] T. O. Reiss, N. Khaneja, S. J. Glaser, Time-optimal coherence-order-selective transfer of in-phase coherence in heteronuclear IS spin systems, *J. Magn. Reson.* **154**, 192-195 (2002).
- [27] N. Khaneja, F. Kramer, S. J. Glaser, Optimal experiments for maximizing coherence transfer between coupled spins, *J. Magn. Reson.* **173**, 116-124 (2005).
- [28] N. Khaneja, T. Reiss, C. Kehlet, T. Schulte-Herbrüggen, S. J. Glaser, Optimal control of coupled spin dynamics: Design of NMR pulse sequences by gradient ascent algorithms, *J. Magn. Reson.* **172**, 296-305 (2005).
- [29] T. E. Skinner, T. O. Reiss, B. Luy, N. Khaneja, S. J. Glaser, Application of optimal control theory to the design of broadband excitation pulses for high resolution NMR, *J. Magn. Reson.* **163**, 8-15 (2003).
- [30] T. E. Skinner, T. O. Reiss, B. Luy, N. Khaneja, S. J. Glaser, Reducing the duration of broadband excitation pulses using optimal control with limited rf amplitude, *J. Magn. Reson.* **167**, 68-74 (2004).
- [31] T. E. Skinner, T. O. Reiss, B. Luy, N. Khaneja, S. J. Glaser, Tailoring the optimal control cost function to a desired output: Application to minimizing phase errors in short broadband excitation pulses, *J. Magn. Reson.*, **172**, 17-23 (2005).
- [32] K. Kobzar, T. E. Skinner, N. Khaneja, S. J. Glaser, B. Luy, Exploring the limits of broadband excitation and inversion pulses, *J. Magn. Reson.* **170**, 236-243 (2004).
- [33] K. Kobzar, B. Luy, N. Khaneja, S. J. Glaser, Pattern pulses: Design of arbitrary excitation profiles as a function of pulse amplitude and offset, *J. Magn. Reson.* **173**, 229-235 (2005).

- [34] C. Kehlet, A. C. Sivertsen, M. Bjerring, T. O. Reiss, N. Khaneja, S. J. Glaser, N. C. Nielsen, Improving solid-state NMR dipolar recoupling by optimal control, *J. Am. Chem. Soc.* **126**, 10202-10203 (2004).
- [35] T. Vosegaard, C. Kehlet, N. Khaneja, S. J. Glaser, N. C. Nielsen, Improved excitation schemes for multiple-quantum magic-angle spinning for quadrupolar nuclei designed using optimal control theory, *J. Am. Chem. Soc.* **127**, 13768-13769 (2005).
- [36] C. Kehlet, T. Vosegaard, N. Khaneja, S. J. Glaser, N. C. Nielsen, Low-power homonuclear dipolar recoupling in solid-state NMR developed using optimal control theory, *Chem. Phys. Lett.* **414**, 204-209 (2005).
- [37] T. Schulte-Herbrüggen, A. Spörl, N. Khaneja, S. J. Glaser, Optimal control-based efficient synthesis of building blocks of quantum algorithms seen in perspective from network complexity towards time complexity, *Phys. Rev. A* **72**, 042331/1-7 (2005).
- [38] D. J. Tannor, S. A. Rice, Control of selectivity of chemical reaction via control of wave packet evolution, *J. Chem. Phys.* **83**, 5013-5018 (1985).
- [39] S. Shi, H. Rabitz, Quantum mechanical optimal control of physical observables in microsystems, *J. Chem. Phys.* **92** 364- 376 (1990).
- [40] W. Jakubetz, E. Kades, J. Manz, State-selective excitation of molecules by means of optimized ultrashort infrared laser pulses, *J. Phys. Chem.* **97**, 12609-12619 (1993).
- [41] Y. Ohtsuki, G. Turinici, H. Rabitz, Generalized monotonically convergent algorithms for solving quantum optimal control problems, *J. Chem. Phys.* **120**, 5509-5517 (2004).
- [42] L. González, K. Hoki, D. Kroner, A. S. Leal, J. Manz, Y. Ohtsuki, Selective preparation of enantiomers by laser pulses: From optimal control to specific pump and dump transitions, *J. Chem. Phys.* **113**, 11134-11142 (2000).
- [43] H. Rabitz, R. de Vivie-Riedle, M. Motzkus, K. Kompa, Whither the future of controlling quantum phenomena?, *Science* **288**, 824-828 (2000).
- [44] C. M. Tesch, L. Kurtz, R. de Vivie-Riedle, Applying optimal control theory for elements of quantum computation in molecular systems, *Chem. Phys. Lett.* **343**, 633-641 (2001).
- [45] S. Conolly, D. Nishimura, A. Macovski, Optimal control solutions to the magnetic resonance selective excitation problem, *IEEE Trans. Med. Imag.* **MI-5**, 106115 (1986).

- [46] J. Mao, T. H. Mareci, K. N. Scott, E. R. Andrew, Selective inversion radiofrequency pulses by optimal control, *J. Magn. Reson.* **70**, 310318 (1986).
- [47] D. Rosenfeld, Y. Zur, Design of adiabatic selective pulses using optimal control theory, *Magn. Reson. Med.* **36**, 401409 (1996).
- [48] O. W. Sørensen, Polarization transfer experiments in high-resolution NMR spectroscopy, *Prog. NMR Spectrosc.* **21**, 503-569 (1989).
- [49] S. J. Glaser, T. Schulte-Herbrüggen, M. Sieveking, O. Schedletsky, N. C. Nielsen, O. W. Sørensen and C. Griesinger, Unitary control in quantum ensembles, maximizing signal intensity in coherent spectroscopy, *Science* **280**, 421-424 (1998).
- [50] E. Chiarparin, P. Pelupessy, G. Bodenhausen, Selective cross-polarization in solution state NMR, *Mol. Phys.* **95**, 759-767 (1998).
- [51] P. Pelupessy, E. Chiarparin, Hartmann-Hahn polarization transfer in liquids: An ideal tool for selective experiments, *Concepts Magn. Reson.* **12**, 103-124 (2000).
- [52] N. Khaneja, T. Reiss, B. Luy, S. J. Glaser, Optimal control of spin dynamics in the presence of relaxation, *J. Magn. Reson.* **162**, 311-319 (2003).
- [53] D. Stefanatos, N. Khaneja, S. J. Glaser, Optimal control of coupled spins in presence of longitudinal relaxation, *Phys. Rev. A* **69**, 022319 (2004).
- [54] N. Khaneja, B. Luy, S. J. Glaser, Boundary of quantum evolution under decoherence, *Proc. Natl. Acad. Sci. USA* **100**, 13162-13166 (2003).
- [55] D. Stefanatos, N. Khaneja, S. J. Glaser, Relaxation optimized transfer of spin order in Ising chains, *Phys. Rev. A* **72**, 062320/1-6 (2005).
- [56] A. J. Shaka, C. J. Lee, A. Pines, Iterative schemes for bilinear operators; application to spin decoupling, *J. Magn. Reson.* **77**, 274-293 (1988).

Figure Captions

Figure 1: Example of a numerically optimized pulse sequence, consisting of the six control amplitudes $u_{1x}(t)$, $u_{1y}(t)$, $u_{2x}(t)$, $u_{2y}(t)$, $u_{3x}(t)$, and $u_{3y}(t)$ with a total duration $\tau = 0.32 J_{12}^{-1}$. The pulse sequence was digitized in 200 time steps of duration $\Delta\tau = 0.016 J_{12}^{-1}$.

Figure 2: Example of a TOP (time-optimal pulse) curve for the case $J_{13} = J_{23} = -2.4J_{12}$, representing numerically optimized transfer amplitudes T_{12} as a function of transfer time τ . The optimum transfer efficiency η^{OC} (dotted line) is defined as the maximum of the exponentially damped TOP curve (dashed curve, c.f. Eq. 11).

Figure 3: In a system consisting of three isotropically coupled spins 1/2, the numerically optimized transfer efficiencies (A) η^{OC} , (B) η^{TOCSY} , (C) η^{TACS} , and (D) $\eta^{two-step}$ are shown for polarization transfer $I_{1z} \rightarrow I_{2z}$.

Figure 4: Cross sections of the transfer efficiency maps shown in Fig. 3 for (A) $J_{13} = J_{23}$, $J_{12} = 1$ Hz, (B) $J_{13} = -J_{23}$, $J_{12} = 1$ Hz.

Figure 5: The optimal transfer time τ_{max} for the damped TOP curves is shown in units of J_{12}^{-1} as a function of J_{13}/J_{12} and J_{23}/J_{12} .

Figure 6: (A) Simulated (solid symbols and smooth curves) and experimental (open symbols) polarization transfer amplitudes T_{12} as a function of the transfer time τ for the homonuclear ^{13}C spin system of fully ^{13}C labelled alanine. Spins I_1 , I_2 , and I_3 correspond to C_β , C' , and C_α , respectively. Solid curve: ideal TOP curve for six spin-selective and unlimited control amplitudes, c.f. Eqs. (7) and (8). Dashed curve: more realistic TOP curve based on two non-selective and unlimited control amplitudes u_x and u_y , c.f. Eq. (5). Solid and open circles: theoretical and experimental transfer amplitudes for optimal control based, purely phase-modulated pulse sequences with a constant rf amplitude of 10.125 kHz optimized for offset variations of ± 170 Hz and rf inhomogeneity. Solid and open squares: simulated and experimental TOCSY transfer amplitudes for DIPSI-2 with a constant rf amplitude of 10.125 kHz. The simulated TOCSY transfer amplitudes (solid squares) are connected by a smooth curve (dash-dotted curve) to guide the eye. (B) Sections of experimental spectra showing the C' signal of alanine after polarization transfer from the C_β . The duration τ of

the transfer sequence is given in multiples of the DIPSI-2 cycle time $\tau_c = 2.84$ ms. Dashed spectra correspond to DIPSI-2 transfer and solid spectra correspond to optimal control based practical polarization transfer sequences.

Figure 7: (A) Non-periodic phase modulation $\varphi(t)$ of a pulse sequence with a constant rf amplitude of 10.125 kHz and duration $\tau = 19.9$ ms optimized for rf inhomogeneity and offset variations of ± 170 Hz around the offsets of ^{13}C spins of alanine at a ^{13}C transmitter frequency of 62.5 MHz. (B) Periodic phase modulation of a conventional DIPSI-2 mixing sequence also with a constant rf amplitude of 10.125 kHz and a total mixing time of 19.9 ms. Each of the seven DIPSI-2 cycles (separated by vertical dotted lines) has a duration of 2.84 ms.

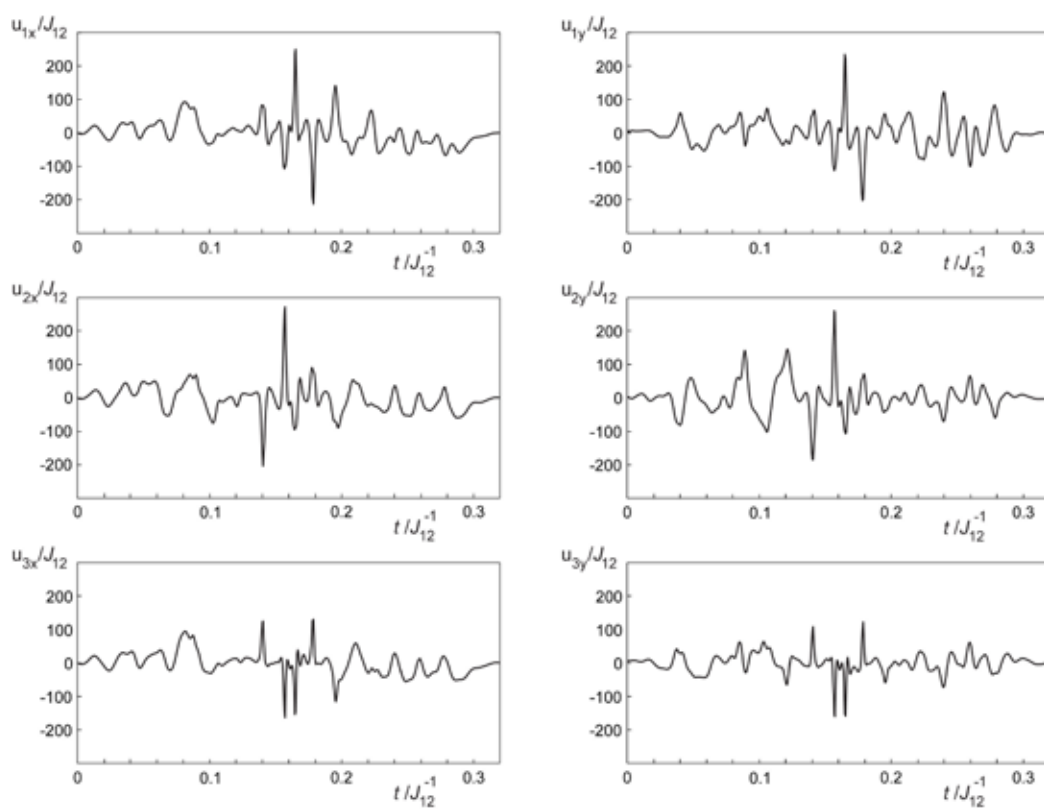


Figure 1

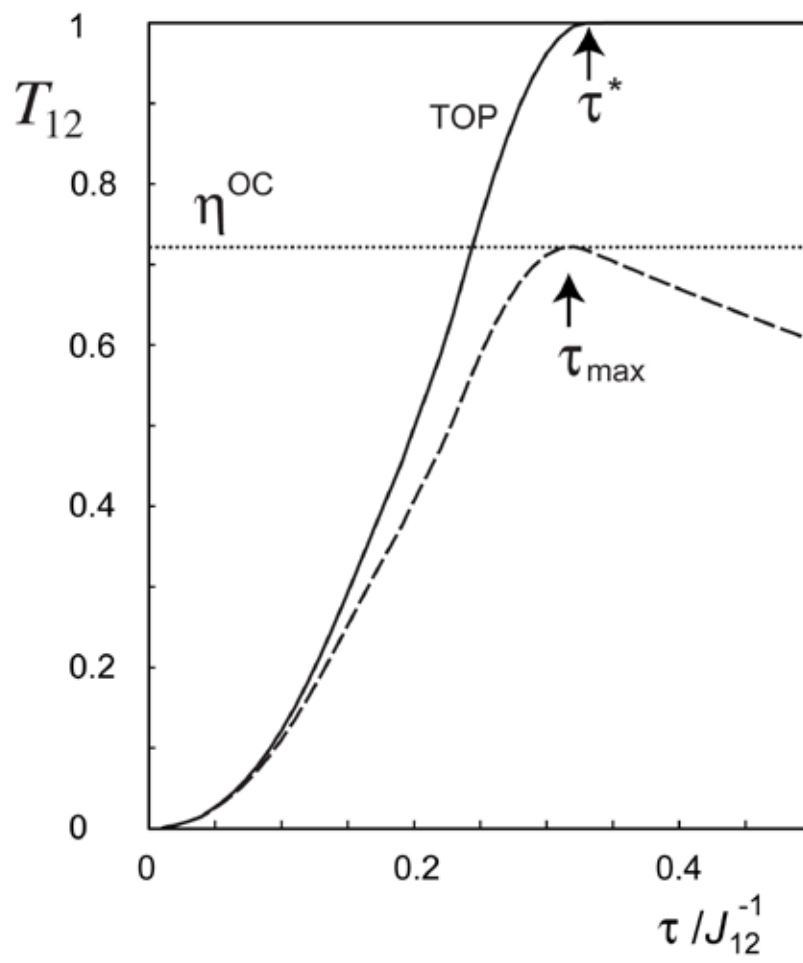


Figure 2

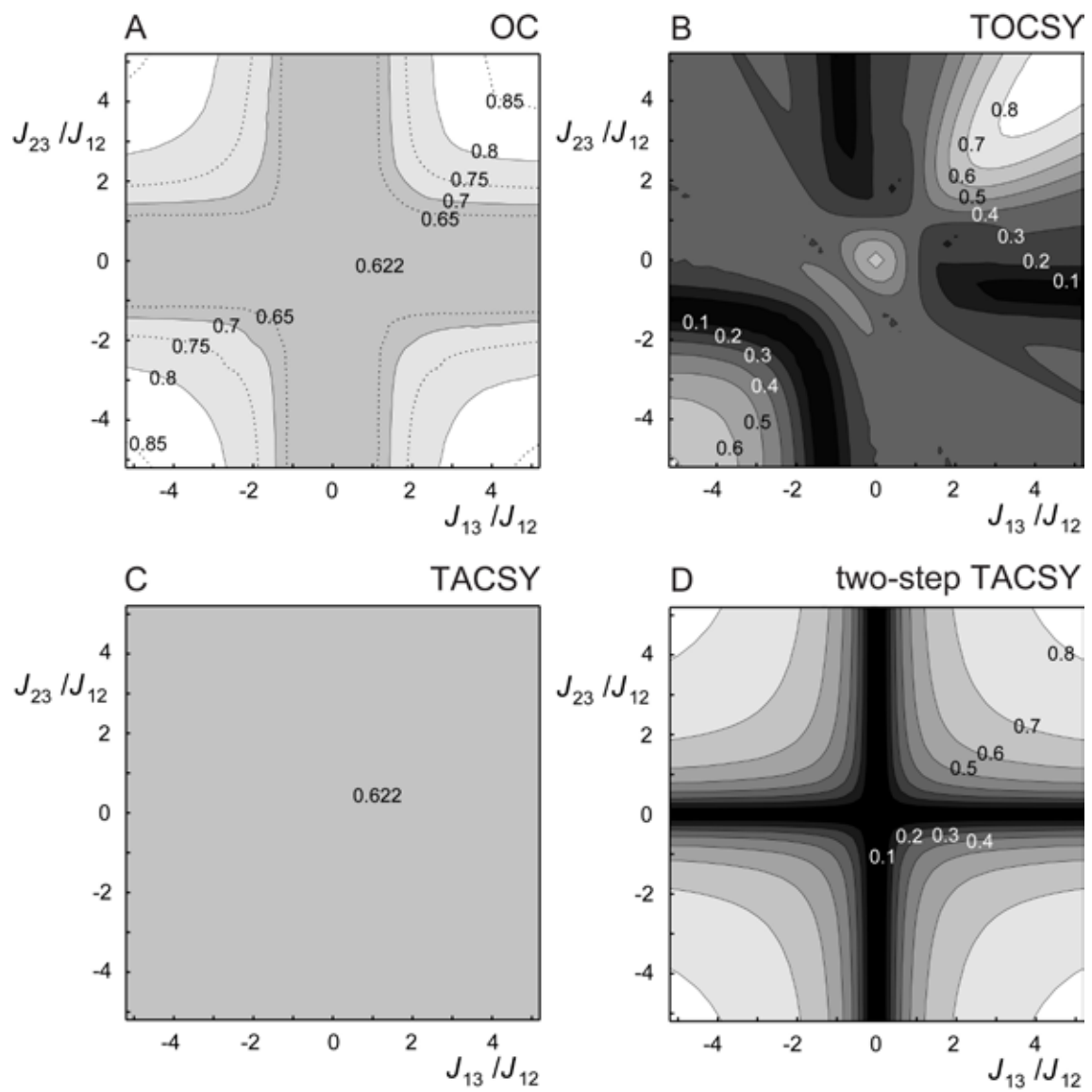


Figure 3

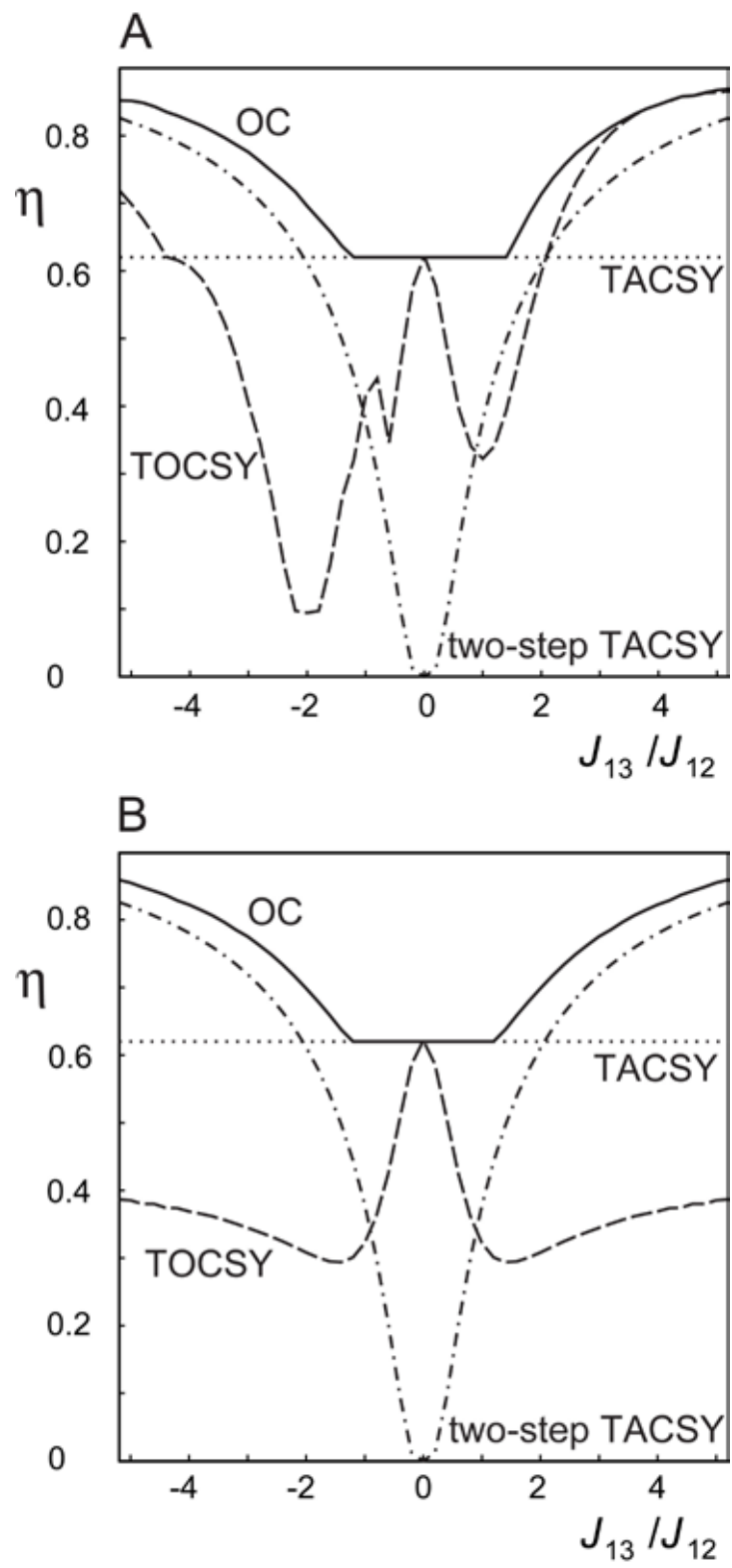


Figure 4

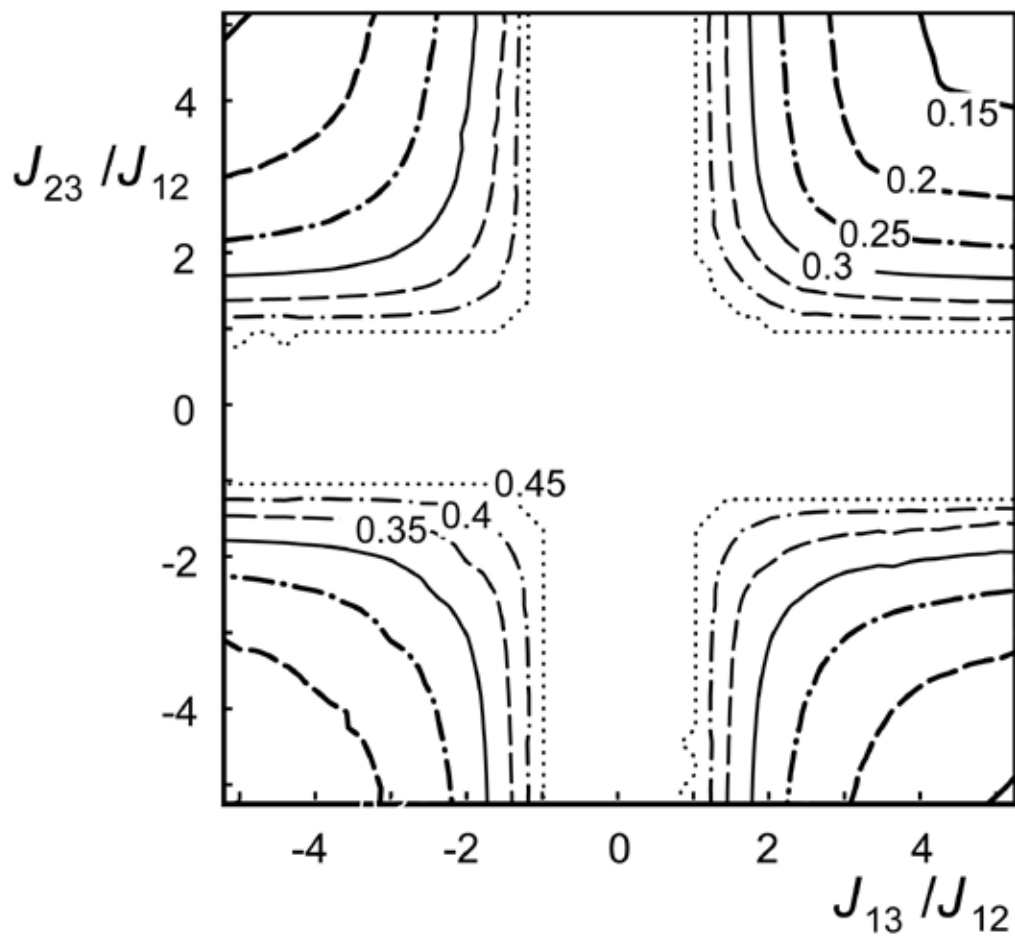


Figure 5

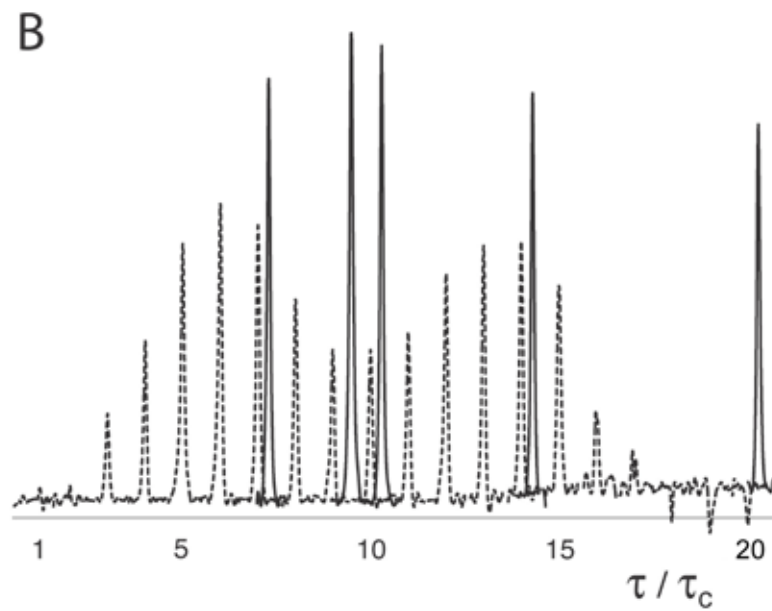
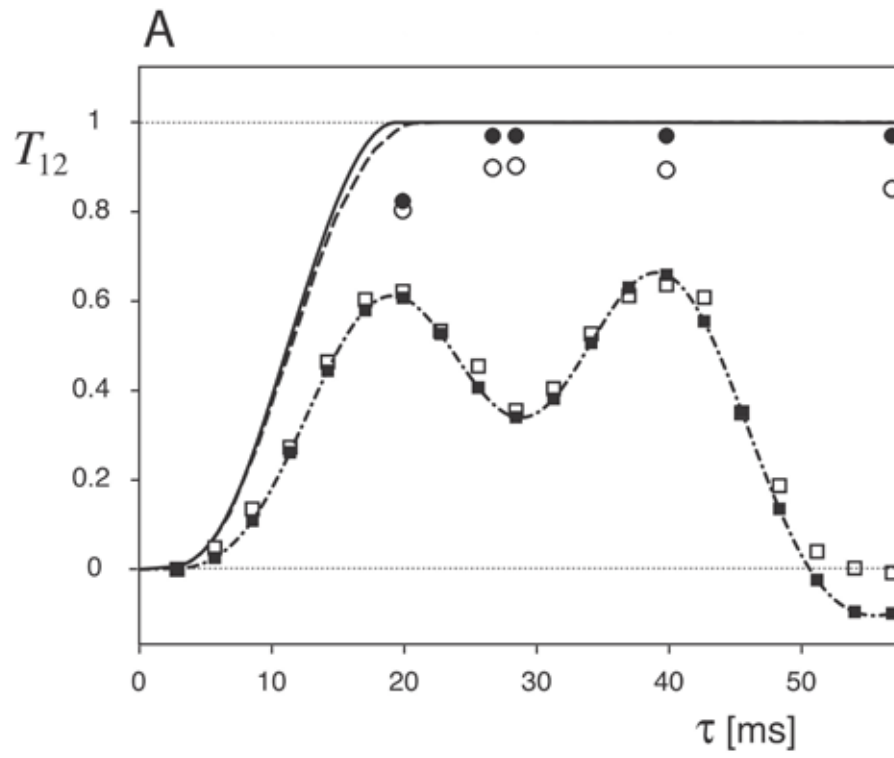


Figure 6

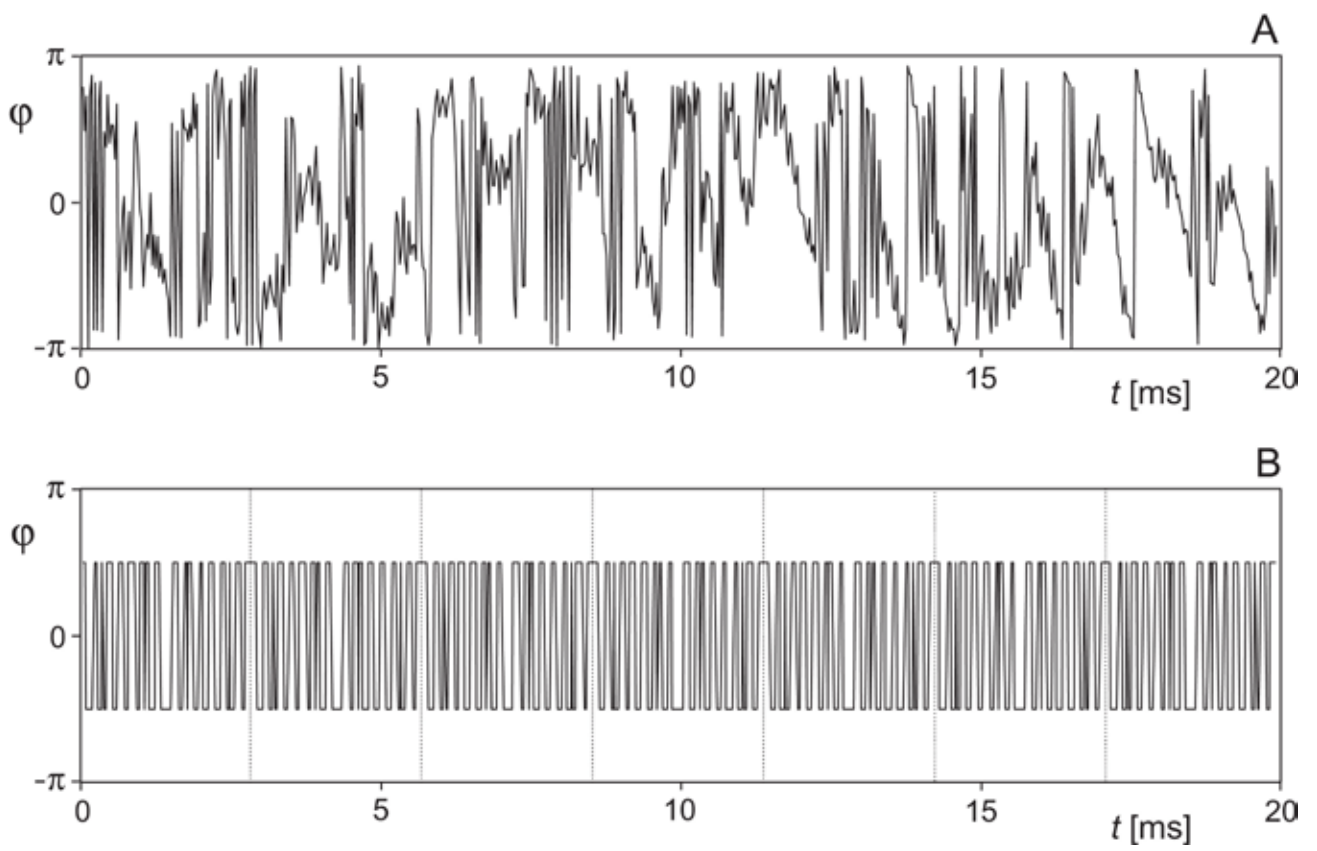


Figure 7